Inorganic Chemistry

Article

pubs.acs.org/IC

Single-Source Precursors for Alloyed Gold−Silver Nanocrystals - A Molecular Metallurgy Approach

David Zopes, Corinna Hegemann, Johannes Schläfer, Wieland Tyrra, and Sanjay Mathur*

Institute of Inorganic Chemistry, University of Cologne, Greinstrasse 6, Cologne, 50939, Germany

Supporting Information

ABSTRACT: Multiple silver(I)-aurates(I) have been prepared by salt metathesis reactions that act as efficient single-source precursors to colloidal gold silver alloys with the highest possible atom economy in the chemical synthesis of nanostructures. The CF_3 group present on the Au cation acts as an in situ reducing agent and can be converted into CO ligands by simple hydrolysis. This ligand-mediated activation and subsequent decomposition of metal−organic precursors impose a molecular control over the nucleation process, producing homogeneously alloyed (Ag−Au) nanoparticles with an atomic Au:Ag ratio of 1:1. The concept also works for the Au−Cu system and acts as a pointer to replace Au (Ag) with less expensive (Cu) metals.

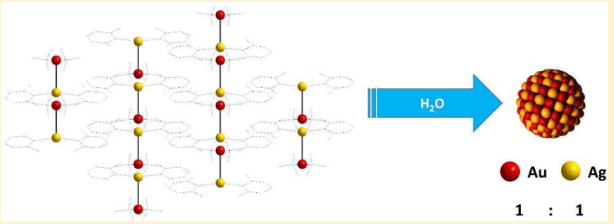

Gold nanoparticles (Au NPs) continue to fascinate the field of nanotechnology,[1,2] mainly due to their appealing optical properties and straightforward synthesis procedures, which have already become a historical landmark in the research on metal colloids.[3] Today, Au NPs find applications in various fields ranging from catalysis to nanomedicine.[2] On the other hand, silver nanoparticles (Ag NPs) are the focus of investigations due to their outstanding properties in the field of medicinal and pharmaceutical applications especially with respect to their antimicrobial activity.[4] The tremendous interest in silver as well as gold particles in modern nanotechnology emerges from their fundamentally new properties spreading over many domains including catalysis,[5] plasmonics,[6] biosensors,[7,8] and medicine.[2,7,8] The last decade has witnessed an ever-growing interest in gold−silver alloy nanoparticles (Au−Ag alloy NPs),[9] due to their miscibility over the entire range, which enables one to enhance their optical[6,9] and catalytic properties[10] by changing their composition, when compared to corresponding monometallic colloids. Commonly, Au−Ag alloy nanoparticles are synthesized by simultaneous reduction of water-soluble silver ($AgNO_3$, $AgCH_3COO$) and gold compounds (in most cases, $HAuCl_4$) by reducing reagents like sodium citrate,[11,12] sodium borohydride,[13] or polyol.[14] The quest for synthetic recipes allowing reproducible syntheses of noble metal nanoparticles with precise control over size, shape, and chemical composition has led to several modifications, whereby the majority of the efforts are directed toward understanding the influence of growth parameters such as reaction time, nature, and concentration of reducing agent,[2,14] as well as reduction and growth kinetics on the resulting nanoparticles (e.g., by addition of capping agents and seed-mediated growth).[2,13−15] Recently, a publication by Swihart et al. described a method to obtain well-dispersed Au−Ag alloy nanoparticles by using chloroauric acid and silver acetate in a hot injection method.[15] So far, development of new molecular sources, especially single-source or halide-free precursors[16,17] for a chemically driven growth of Au−Ag alloy nanoparticles, has been less investigated despite the influence of the halide ions as disturbing capping reagents well-studied in the case of gold nanoparticles.[17−19] Fundamentally, the synthesis of nanoscopic alloy particles with homogeneous compositions is a synthetic challenge due to the differential decomposition behavior of the individual precursors and intrinsic tendency for phase separation present during the nucleation phase.[20,21] We have earlier reported on the chemical implications of molecular sources in homogenizing the particle growth by suppressing the diffusion-driven growth due to the pre-existent chemical bonds between the phase-forming elements.

We report here a new class of stable bimetallic Ag−Au precursors enabling molecular metallurgy of Au−Ag nanoparticles with very high atom economy. Recently, we reported on the hydrolytic decomposition of bis(trifluoromethyl)aurate(I), $[NMe_4][Au(CF_3)_2]$, as a highly controllable pathway to obtain monodispersed "naked" gold nanoparticles in aqueous solutions.[22] The presence of chlorides or any other coordinating species on the particle's surface could be excluded by XPS measurements. The decomposition mechanism was elucidated by ^{19}F NMR experiments giving evidence for an intermediately formed trifluoromethyl-gold carbonyl species.[22] The proposed mechanism with in situ formed CO as reducing agent leading to Au(0) and CO_2 was confirmed by an outstanding contribution by Martinez-Salvador et al.[23] by isolating and characterizing the intermediate species, $[Au(CF_3)(CO)]$, formed in the decomposition process. Already in 1905, Donau claimed CO to be a reagent to convert $AuCl_4^-$ into red colloidal gold.[24] Herein, we report a new class of

Received: December 13, 2014
Published: April 9, 2015

DOI: 10.1021/ic502924s
Inorg. Chem. 2015, 54, 3781−3787

Scheme 1. Reaction Procedure To Synthesize Phosphane-Stabilized Silver(I)-aurates(I)

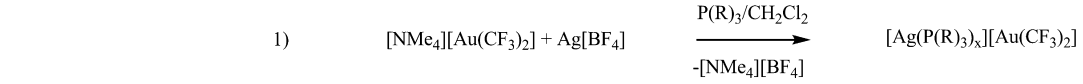

bimetallic Au−Ag complexes of the general formula $[Ag(L)_2][Au(CF_3)_2]$, obtained selectively in the salt metathesis reaction of Ag^+ salts and $[NMe_4][Au(CF_3)_2]$ (L = 2,6-dimethylpyridine (Lut), 2,2 bipyridine (Bipy), dimethylaminopyridine (DMAP), and pyridine (Py)). Further, the hydrolytic decomposition of new silver-aurates in a fast and facile microwave process led to compositionally pure Au−Ag alloy nanoparticles with homogeneous sizes, shapes, and high stability.

Syntheses of Silver(I)-aurates (I). We have earlier reported on the crystal structure and a convenient synthesis of $[NMe_4][Au(CF_3)_2]$[22] that opened new opportunities to rationally construct bimetallic assemblies by making use of the rather low solubility of $[NMe_4][BF_4]$ in CH_2Cl_2 (eq 1). To elucidate our mechanistic model and to confirm the intermediate formation of a silver(I)-aurate(I), we performed reactions in the presence of phosphine ligands (eq 1), which are known to be less light-sensitive (Scheme 1).

The compounds $[Ag(TPP)_4][Au(CF_3)_2]$ and $[Ag(P(^tBu)_3)_2][Au(CF_3)_2]$ were obtained in high yields (~95%) and purity and showed, in both the cases, a high stability against humidity and especially against visible light irradiation.

Crystals of $[Ag(TPP)_4][Au(CF_3)_2]$ suitable for crystallographic analysis were obtained out of a CH_2Cl_2 solution kept at 7 °C. The solid-state structure (Figure 1a) showed a tetrahedral arrangement of four TPP ligands around the Ag^+ ion. The angles between metal center and ligands (P(1)−Ag(1)−P(3) = 108.73(5)°, P(1)−Ag(1)−P(4) = 110.61(5)°, P(3)−Ag(1)−P(4) = 108.75(4)°, P(1)−Ag(1)−P(2) = 109.04(5)°, P(3)−Ag(1)−P(2) = 110.06(4)°, and P(4)−Ag(1)−(2) = 109.63(4)°) exhibited minimal deviation (<1%) from the ideal value of 109.5°. The average length of Ag−P bonds (263.2 pm) was in good agreement with values observed in $[Ag(PPh_3)_4)]\cdot SbF_6\cdot CHCl_3$.[25] Expectedly, the Au^+ ion is nearly linear, coordinated by two trifluoromethyl ligands (C2−Au1−C1 = 178.7(4)°) with observed bond lengths (201.6 and 201.9 pm) being significantly shorter than those found in $[PNP][Au(CF_3)_2]$ (206.6 pm),[22] possibly due to the steric demands of the TPP ligands, which also explained the observed separation between gold and silver units in the elementary cell (Figure 1a and the Supporting Information for the crystal packing).

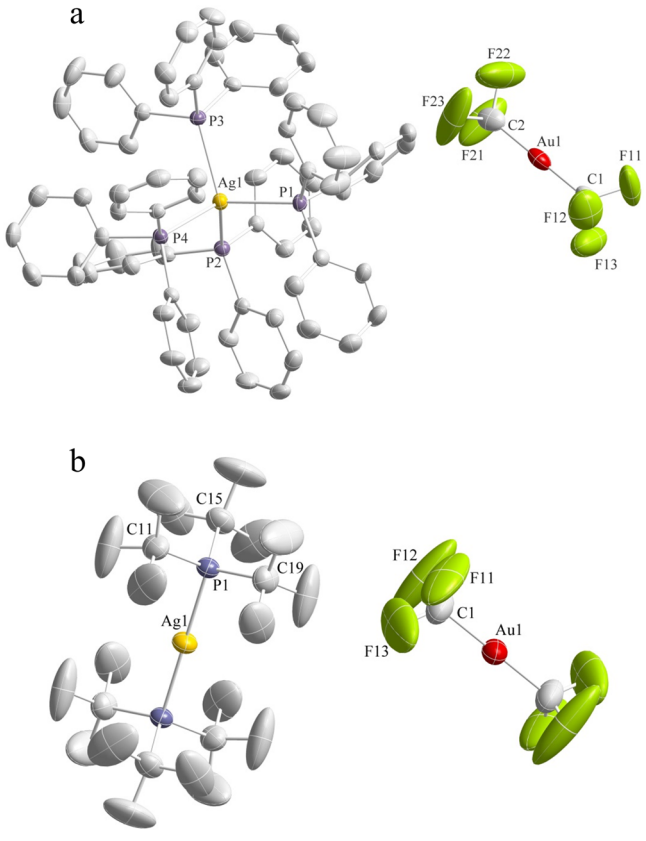

Figure 1. Molecular structures of (a) $[Ag(TPP)_4][Au(CF_3)_2]$ and (b) $[Ag(P(^tBu)_3)_2][Au(CF_3)_2]$. The displacement ellipsoids are drawn at 50% probability level; hydrogen atoms are omitted for clarity.

In this case, a chemical interaction between metallic centers can be excluded. Crystals of $[Ag(P(^tBu)_3)_2][Au(CF_3)_2]$ were isolated out of a THF solution kept at −30 °C. The molecular structure (Figure 1b) displayed a linear coordination for silver as well as for gold with metal−ligand angles being 180.00(3)°. For the linear coordination, the Ag−P bonds have characteristic average bond lengths of 239.4 pm[26] and are shorter than those reported for $[Ag(TPP)_4][Au(CF_3)_2]$. The Au−C bonds (200.5 pm) are comparable with the familiar TPP-derivative. The structure (Figure 1b; see the Supporting Information for the crystal packing) showed ionogenic gold and silver units due to the sterically demanding phosphine ligand with no pronounced Ag−Au interactions.

The ^{31}P NMR spectrum of $[Ag(TPP)_4][Au(CF_3)_2]$ indicated a fast exchange of the triphenylphosphine (TPP) ligand in solution at room temperature, leading to only one strongly broadened signal with a chemical shift at +8.3 ppm. Cooling the sample down to 200 K decelerates the exchange and two coordination states of the Ag^+ ions (tri- (+8.6 ppm; $^1J_{Ag,P}$ 448 Hz) and tetra- (+5.2 ppm; $^1J_{Ag,P}$ 240 Hz) coordinated) could be observed (see Figure 2a and the Supporting Information).[1] Signals could be attributed by their chemical shifts and their $^1J_{Ag,P}$ coupling values reported by Alyea et al.[27] The $^{31}P,^{109}Ag$-HMQC-NMR experiment carried out at 200 K (optimized for a ^1J coupling of 240 Hz) enabled us to determine the chemical shift of the Ag^+ ion at +1145 ppm (Figure 2a). The ^{19}F NMR spectrum showed a sharp signal with a chemical shift of −26.2 ppm, indicating no interaction of Ag and Au units in solution. The ^{31}P NMR spectrum of the second silver-phosphine aurate, $[Ag(P(^tBu)_3)_2][Au(CF_3)_2]$, showed a sharp signal at room temperature with a chemical shift of +81 ppm (Figure 2b and the Supporting Information). Hereby, a ligand exchange in solution, such as observed for $[Ag(TPP)_4][Au(CF_3)_2]$, can be excluded. Chemical shifts as well as $^1J_{Ag,P}$ coupling values (^{107}Ag−P 441 Hz and ^{109}Ag−P 511 Hz) verified a linear coordination of the Ag^+ ion in solution as observed in the solid state.[28] The chemical shift of the Ag^+ ion in the $^{31}P,^{109}Ag$ HMQC NMR spectrum was observed in the upfield range (+580 ppm) when compared to the TPP derivative (Figure 2b).

DOI: 10.1021/ic502924s
Inorg. Chem. 2015, 54, 3781−3787

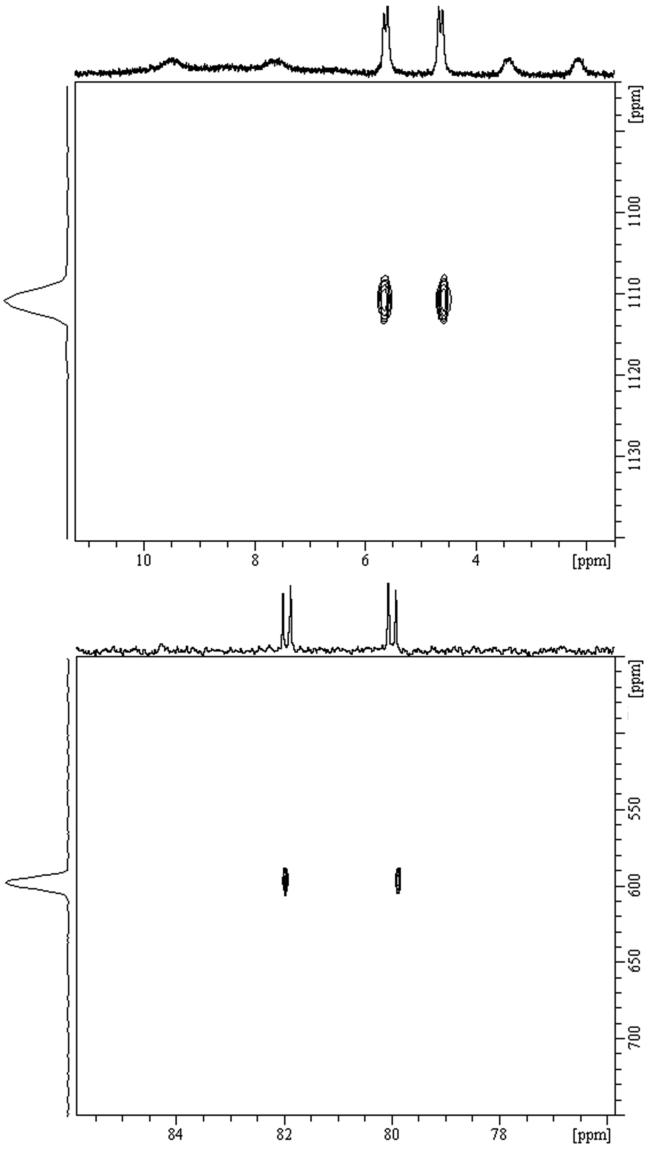

Figure 2. $^{31}P,^{109}Ag$-HMQC-NMR experiments of (a) $[Ag(TPP)_4][Au(CF_3)_2]$ in CD_2Cl_2 at 200 K (optimized for a ^1J coupling of 240 Hz) and (b) for $[Ag(P(^tBu)_3)_2][Au(CF_3)_2]$ in $CDCl_3$ at room temperature (optimized for a ^1J coupling of 500 Hz).

In a two-step reaction procedure (eqs 2 and 3, Scheme 2), various silver(I)-aurates(I) with different nitrogen-based ligands (N-ligand) were synthesized. The first step included a facile synthesis of $[Ag(N\text{-ligand})_2][BF_4]$, which were used in the second step as educts together with $[NMe_4][Au(CF_3)_2]$ to form $[Ag(N\text{-ligand})_2][Au(CF_3)_2]$ and insoluble $[NMe_4][BF_4]$ as byproduct. Fernandez and co-workers synthesized under comparable reaction conditions the bimetallic complex $[Ag(Py)_3][Au(C_6F_5)_2]\cdot Py$ starting from $AgClO_4$ and $[N(^nBu)_4][Au(C_6F_5)_2]$.[29]

The silver species, $[Ag(N\text{-ligand})_2][BF_4]$ (step 1, Scheme 2), were obtained as powders in quantitative yields and high purity. A comprehensive characterization (NMR, CHNS, IR) is given in the Supporting Information. These compounds are stable against daylight and humidity and could be stored and handled under ambient conditions. The silver(I)-aurates(I), $[Ag(N\text{-ligand})_2][Au(CF_3)_2]$, obtained are listed in Table 1. All of them were synthesized in an analytically pure state and good yields (80−90%) as light-sensitive powders. In a foregoing publication, we already reported about the light-induced controlled oxidation of the aurate anion into the Au(+II)-species, $[(CF_3)_4Au_2(Py)_2]$.[30] Table 1 provides an overview about synthesized $[Ag(N\text{-ligand})_2][Au(CF_3)_2]$ compounds and their chemical shifts observed in ^{109}Ag, ^{15}N, and ^{19}F NMR experiments. The corresponding ^1H and ^{13}C chemical shifts are given in the Supporting Information. The NMR signals in all the cases were sharp with the exception of $[Ag(DMAP)_2][Au(CF_3)_2]$, where broadened signals of the aromatic protons signifying interactions in solution were observed.

The ^{15}N NMR shifts of investigated $[Ag(N\text{-ligand})_2][Au(CF_3)_2]$ compounds (Table 1) were detected by $^1H,^{15}N$ HSQC experiments with individual coupling constants (3−11 Hz) and underline the coordination through a strong high field shift. These results are in good agreement with values observed by Kleinmaier et al.[31] Although silver and gold are members of the same group 10 and trifluoromethyl derivatives are known in the oxidation state +1 for both, no evidence was found in the ^{19}F NMR spectrum (δ: −28 ppm (Table 1)) for any interaction between $[(CF_3)Ag]$[32] and $[(CF_3)Au]$[22] derivatives and neither ^{19}F nor ^{13}C NMR spectra nor ^{19}F- or ^{13}C-$^{107/109}Ag$ couplings showed any line broadening. The observed ^{13}C satellites of the ^{19}F signal showed a $^1J_{CF}$ coupling of 347 Hz, which is a typical value for Au(+I) species and is in good agreement with the published value for $[NMe_4][Au(CF_3)_2]$.[22] The ^{109}Ag chemical shifts could be detected for all compounds with sharp signals found in a typical range (350−500 ppm) for linear coordinated Ag(I) species by a N-donor ligand, like reported by Jucker and co-workers.[33] The authors also pointed out that the shift

Scheme 2. Two-Step Reaction Procedure To Synthesize N-Ligand Stabilized Silver(I)-aurates(I)

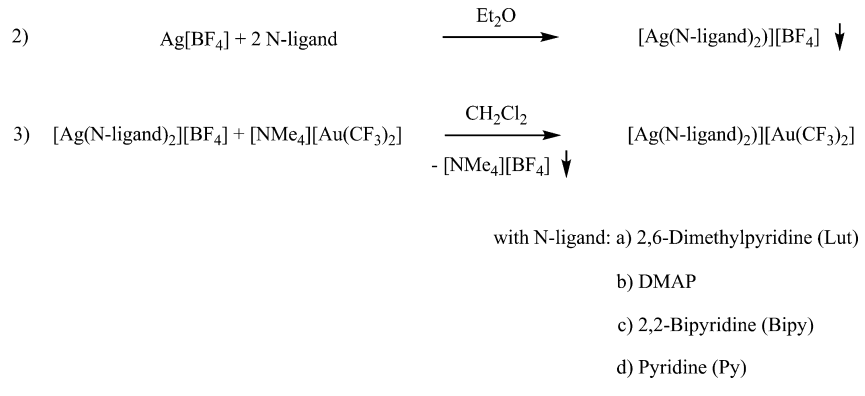

DOI: 10.1021/ic502924s
Inorg. Chem. 2015, 54, 3781−3787

Table 1. Synthesized $[Ag(N\text{-ligand})_2][Au(CF_3)_2]$ Compounds and Their NMR Chemical Shifts (^{109}Ag, ^{15}N, and ^{19}F) at Room Temperature

compound	solvent	chemical shifts (in ppm)		
		^{109}Ag	^{15}N (free ligand)	^{19}F
$[Ag(Lut)_2][Au(CF_3)_2]$	CD_3CN	404 (s)[a]	288 (315)	−28.6 (s)
$[Ag(DMAP)_2][Au(CF_3)_2]$	CD_3CN	411 (s)[a]	220[b] (275)	−28.6 (s)
$[Ag(Bipy)_2][Au(CF_3)_2]$	CD_3CN	491 (s)[a]	284 (308)	−28.6 (s)
$[Ag(Py)_2][Au(CF_3)_2]$	CD_2Cl_2	404 (s)[a]	260[b] (316)	−28.1 (s)

[a]Sharp Signal. [b]Detected from respective $[Ag(N\text{-ligand})_2][BF_4]$ derivative.

depends on the Ag(I) concentration and the formation of a linear coordinated silver complex like $[Ag(Py)_2]^+$ appears to be thermodynamically preferred.[33] Therefore, the obtained molecular species must be seen as $[Ag(I)(N\text{-ligand})_2][Au(I)(CF_3)_2]$ in solution.

The molecular structure (Figure 3) of the derivative $[Ag(Lut)_2][Au(CF_3)_2]$ provided convincing evidence of an

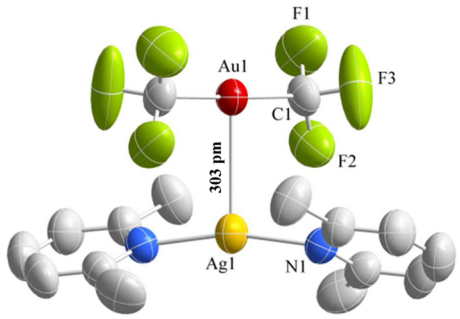

Figure 3. Molecular structure of $[Ag(Lut)_2][Au(CF_3)_2]$. The displacement ellipsoids are drawn at 50% probability level; H atoms are omitted for clarity.

intermetallic bond (303 pm) between gold and silver, as reported by Uson et al. for $(F_5C_6)_2Au(\mu\text{-}AgSC_4H_8)_2Au(C_6F_5)_2$.[34] The Au−C bonds (207.1 and 198.3 pm) as well as the nearly linear coordination of the gold atom (176.6°) are similar to familiar compounds like $[Ag(TPP)_4][Au(CF_3)_2]$, $[Ag(P(^tBu)_3)_2][Au(CF_3)_2]$, and $[NMe_4][Au(CF_3)_2]$.[22]

The Ag−N bonds (216.0 and 214.1 pm) have characteristic values for doubly coordinated silver(I) species by nitrogen-based aromatic ligands, as reported for $[Ag(DMAP)_2]NO_3\cdot 2H_2O$.[35] The N−Ag−N angle (165.5°) clearly deviates from an ideal linear coordination, which can be explained by steric constraints due to the large lutidine ligand and was already observed in different $[Cu(I)(Lut)]^+$ derivatives.[36]

Microwave-Assisted Low-Temperature Pathway to Gold−Silver Alloy Nanoparticles. The hydrolytic decomposition of the molecular silver-aurates can be induced by an interaction of d electrons of gold atom with a σ^* molecular orbital of the C−F bond, which results in the activation of this otherwise very stable bond (Figure 4).[37] The activation of the C−F bond is yet not fully understood. However, the mentioned $d\pi \rightarrow \sigma^*$ interaction is a good explanation for the C−F bond cleavage as well as the preliminary mechanistic investigation of the decomposition of $[NMe_4][Au(CF_3)_2]$.[22]

Consequently, nucleophilic attack by H_2O is able to cleave the C−F bonds with the formation of HF, HF_2^-, and $[Au(CF_3)(CO)]$[23] in a first step, followed by the formation of CO_2 and $[Au(solvent)(CF_3)]$ (Figure 4).[19,22] The in situ formed CO ligands work as reducing agents for Ag(I) and

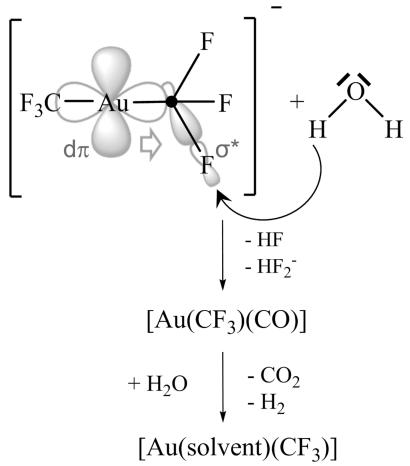

Figure 4. Schematic of $d \rightarrow \sigma^*$ donation of metal d orbitals to C−F antibonding σ orbital as a possible initial step for the C−F bond cleavage and starting point of the hydrolytic decomposition of $[Au(CF_3)_2]^-$ derivatives.

Au(I) and oxidize themselves to CO_2, which could be identified by precipitation of $BaCO_3$ upon bubbling the gas through a $Ba(OH)_2$ solution. All intermediates could be detected by ^{19}F NMR spectroscopy[22] or isolated as molecular species characterized by single-crystal diffraction studies.[23] A complete reaction mechanism of the hydrolytic decomposition is shown in Scheme 3.

The decomposition of the bimetallic precursor could be augmented by adding small amounts of ammonia that reacted with the in situ generated HF to form ammonium fluoride (^{19}F NMR; δ: −119 ppm). For a homogeneous nucleation of alloy particles, the silver-aurates need to be soluble in H_2O that made all $[Ag(N\text{-ligand})_2][Au(CF_3)_2]$ derivatives efficient single-source precursors for gold−silver alloy colloids.

The formation of metallic nanoparticles was confirmed by characteristic surface plasmon resonance and intensive coloration of colloidal solutions obtained after decomposition. Whereas gold nanoparticles in aqueous solutions were red to blue (λ_{max} 515−550 nm; depending on particle's size and shape),[12] silver colloids are yellow to green (λ_{max} 380−420 nm; depending on particle's size and shape),[6] and gold−silver alloy nanoparticles showed a brownish coloration and an absorption maxima centered around 450−475 nm for Au:Ag alloy nanoparticles.[38] In core−shell morphologies, one would expect different absorption maxima, depending on which metal is present in the shell.[39,40] Moreover, the absence of any additional feature in the absorption curve excluded an overlap of two different absorption curves and confirmed the formation of homogeneous colloids. All $[Ag(N\text{-ligand})_2][Au(CF_3)_2]$ compounds listed in Table 1 could be successfully converted into gold−silver alloy nanoparticles by microwave-assisted

DOI: 10.1021/ic502924s
Inorg. Chem. 2015, 54, 3781−3787

Scheme 3. Reaction Procedure for the Hydrolytic Decomposition of $[Ag(N\text{-ligand})_2][Au(CF_3)_2]$

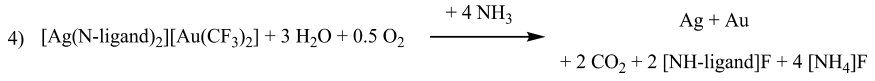

hydrolytic decomposition at 333 K. To prevent the agglomeration of as-formed nanoparticles, 2 mL of an aqueous solution of 1 wt % thiolated PEG (6-mercaptohexan-PEG) was added to 8 mL of the aqueous colloidal solution.

All colloidal solutions displayed absorption maxima in the expected range for alloy nanoparticles with a Ag:Au ratio of 1:1 at 465 ± 2 nm (Figure 5). No additional spectral features were observed and no changes were detected by repeating the absorption measurement in samples stored for a week and longer. TEM images (Figure 6) showed spherical particles with sizes between 2 and 3 nm, and corresponding EDX analyses of the alloy particles confirmed the expected 1:1 ratio of gold and silver (Table 2). Small divergences could be explained by the light sensitivity of silver.[30]

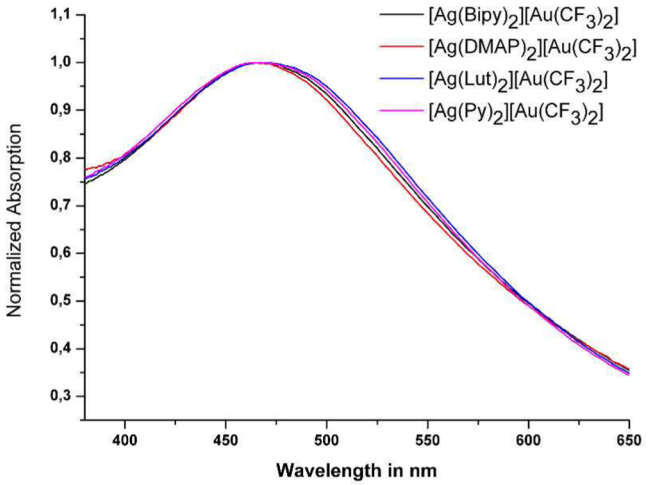

Figure 5. UV/vis absorption measurements of obtained aqueous AgAu alloy colloidal solutions starting from $[Ag(N\text{-ligand})_2][Au(CF_3)_2]$ with N-ligand (a) bipy (black curve), (b) DMAP (red curve), (c) Lut (blue curve), and (d) Py (pink curve).

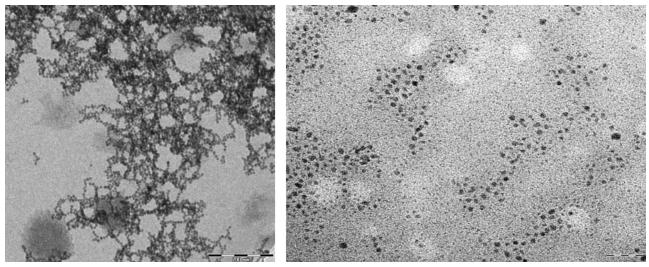

Figure 6. TEM images of as-obtained gold (left) and gold–silver alloy nanoparticles (right) from $[NMe_4][Au(CF_3)_2]$ (left) and $[Ag(Lut)_2][Au(CF_3)_2]$ (right). The poor contrast in the case of alloyed particles is due to their smaller size and consequently smaller diffraction volume in contrast to pure gold nanoparticles.

Similar to the herein reported silver(I)-aurates(I), we have also successfully synthesized copper(I)-aurate(I), $[Cu(CH_3CN)_4][Au(CF_3)_2]$, based on the salt metathesis reaction of $[NMe_4][Au(CF_3)_2]$ and $[Cu(CH_3CN)_4][BF_4]$. The microwave-assisted hydrolytic decomposition of the Au–Cu compound resulted in a blue solution with an absorption maximum at ∼544 nm that corresponds to the mathematical average of the absorption maxima of colloidal gold (∼520 nm)[12] and copper (∼560–570 nm)[42] and suggests the formation of a colloidal Cu–Au alloy. Further characterizations as well as syntheses of other bimetallic gold precursors are in progress.

Table 2. Overview of As-Synthesized Ag–Au Alloy NPs from Different Precursors

compound	size in nm (±)	Ag:Au ratio in atom %
$[Ag(Lut)_2][Au(CF_3)_2]$	2.9 (8%)	49:51
$[Ag(DMAP)_2][Au(CF_3)_2]$	3.2 (12%)	48:52
$[Ag(Bipy)_2][Au(CF_3)_2]$	2.7 (7%)	50:50
$[Ag(Py)_2][Au(CF_3)_2]$	2.8 (6%)	46:54

In summary, the characterizations of structural features and decomposition of the new silver-aurates in solution provide a feasible strategy to control the nucleation of bimetallic nanocrystals and suppress the possible phase segregation. In addition, the activation of the $Au–CF_3$ bond and the consequent attack of water suggest new decomposition pathways that will be of substantial interest in understanding the role of Au compounds in homogeneous catalysis. All $[Ag(N\text{-ligand})_2][Au(CF_3)_2]$ compounds were successfully converted into homogeneous gold–silver alloy nanoparticles with sizes between 2 and 3 nm and close to the ideal Ag:Au ratio of 1:1. Corresponding UV/vis absorption measurements underline their expected Ag:Au ratio and verify the formation of alloyed gold–silver from molecular precursors. Finally, the here demonstrated potential of a molecular metallurgy approach offers a unique opportunity to substitute other nonexpensive metals (e.g., Cu) to obtain next-generation catalysts with high atom economy.

EXPERIMENTAL SECTION

Routine NMR spectra were recorded on a Bruker AVANCE II 300 at 298 K; frequencies (external standards): ^{1}H 300.13 MHz (TMS), ^{13}C 75.5 MHz (TMS), ^{19}F 282.40 (CCl_3F), and ^{31}P 121.49 MHz (H_3PO_4). Positive shifts denote downfield resonances. ^{15}N NMR chemical shifts were detected by $^{1}H,^{15}N$-HSQC-NMR experiments optimized on the respective coupling values (3–11 Hz). ^{109}Ag NMR- and $^{31}P,^{109}Ag$ HMQC NMR experiments were run on a Bruker Avance 400 spectrometer at different temperatures (200–298 K). The spectrometer frequencies are (external standards): ^{1}H 400.13 MHz (TMS), ^{19}F 376.50 MHz (CCl_3F), and ^{109}Ag 18.61 MHz ($AgNO_3$). Elemental analyses were carried out with a HEKAtech Euro EA 3000 apparatus. Data collection for X-ray crystal structure determination for all compounds was performed on a STOE IPDS 2 T diffractometer using graphite-monochromated Mo–Kα radiation (λ = 0.71073 Å). The data were corrected for Lorentz and polarization effects. A numerical absorption correction based on crystal-shape optimization was applied for all data.[41] The programs used in this work are Stoe's X-Area,[42] including X-RED and X-Shape for data reduction and absorption correction,[43] and the WinGX suite of programs,[44] including SIR-92[45] and SHELXL-97[46] for structure solution and refinement. The hydrogen atoms were placed in idealized positions and constrained to ride on their parent atom. The last cycles of refinement included atomic positions for all atoms, anisotropic thermal parameters for all

DOI: 10.1021/ic502924s
Inorg. Chem. 2015, 54, 3781–3787

non-hydrogen atoms, and isotropic thermal parameters for all hydrogen atoms. CCDC 1058317-1058319 contain the supplementary crystallographic data for this paper. These data can be obtained free of charge from The Cambridge Crystallographic Data Centre via www.ccdc.cam.ac.uk/data_request/cif. DTA analyses were done by a STARe system from Mettler Toledo with a TGA/DSC1 unit and the gas controller GC100. For all hydrolytic decomposition processes, we used the microwave system Discover from CEM. Morphology and size of particles were investigated by a TEM Philips CM12 (100 kV) from Fei and a STEM CM300 FEG/UT (300 kV) from Phillips. EDX measurements were measured on the same STEM combined with the analytic system Noran System Seven from Thermo Fisher Scientific. Size distribution based on the TEM images was calculated by ImageJ. Absorption spectroscopic measurements were carried out with a Lambda 300 from PerkinElmer.

$[Ag(PPh_3)_4][Au(CF_3)_2]$. A 0.123 g (1 equiv, 0.3 mmol) portion of $[NMe_4][Au(CF_3)_2]$ was solved in 10 mL of dried methylene chloride under a N_2 atmosphere. Then, 0.058 g (1 equiv, 0.3 mmol) of $Ag[BF_4]$ and hereafter 0.156 g of triphenylphosphine (4 equiv, 1.2 mmol) were added. $[NMe_4][BF_4]$ precipitated instantly as a white precipitate. After 3 h stirring, the reaction was finished and the solution was cooled down to 254 K for a complete precipitation of $[NMe_4][BF_4]$. To obtain the solid white product in nearly quantitative yield, all volatile products were removed carefully under reduced pressure ($1*10^{-2}$ mbar). Colorless crystals could be observed from a THF/CH_2Cl_2 solution at 254 K.

$[Ag(P(^tBu)_3)_2][Au(CF_3)_2]$. A 0.123 g (1 equiv, 0.3 mmol) portion of $[NMe_4][Au(CF_3)_2]$ was solved in 10 mL of dried tetrahydrofuran under an inert atmosphere (glovebox). Then, 0.058 g (1 equiv, 0.3 mmol) of $Ag[BF_4]$ and hereafter 0.6 mL of a 1 M tris(*tert*-butyl)phosphine THF solution (2 equiv, 0.6 mmol) were added. $[NMe_4][BF_4]$ precipitated instantly as an off-white precipitate. After 3 h stirring, the reaction was finished and the solution was cooled down to 243 K for a complete precipitation of $[NMe_4][BF_4]$. To obtain the solid white product in nearly quantitative yield, all volatile products were removed carefully under reduced pressure ($1*10^{-2}$ mbar). Colorless crystals could be obtained from the THF solution at 243 K.

$[Ag(N\text{-}ligand)_2][BF_4]$. One equivalent of $Ag[BF_4]$ was solved under light-protected conditions in diethyl ether. To the well stirred solution, 2.2 equiv of the N-ligand (with N-ligand = 2,6-dimethylpyridine (Lut), 2,2 bipyridine (Bipy), dimethylaminopyridine (DMAP), and pyridine (Py)) was added, and the respective $[Ag(N\text{-}ligand)_2][BF_4]$ precipitated as a white to yellowish powder in nearly quantitative yield. All products were washed three times with diethyl ether to remove all excess of N-ligand.

$[Ag(N\text{-}ligand)_2][Au(CF_3)_2]$. An equimolar amount of $[NMe_4][Au(CF_3)_2]$ (1 equiv) and $[Ag(N\text{-}ligand)_2][BF_4]$ (with N-ligand = 2,6-dimethylpyridine (Lut), 2,2 bipyridine (Bipy), dimethylaminopyridine (DMAP), and pyridine (Py)) (1 equiv) were added to dry methylene chloride. $[NMe_4][BF_4]$ precipitated as white flocculation and could be separated from the colorless solution by inert filtrations. The solvent was carefully evaporated by N_2-influx, and the respective $[Ag(N\text{-}ligand)_2][Au(CF_3)_2]$ derivatives were obtained as a white to white yellowish powder in nearly quantitative yields.

Microwave-Assisted Decomposition of $[Ag(N\text{-}ligand)_2][Au(CF_3)_2]$. Aqueous solutions (0.25 mM) of the respective $[Ag(N\text{-}ligand)_2][Au(CF_3)_2]$ (with N-ligand = 2,6-dimethylpyridine (Lut), 2,2 bipyridine (Bipy), dimethylaminopyridine (DMAP), and pyridine (Py)) were prepared. The mixtures were well-shaken before they were heated up to 60 °C (dynamic mode (25 W) for 90 s in a microwave system. The received particle solutions had a characteristic brown color, and bubbles of the CO_2 byproduct could be observed at the glass wall. Subsequently, 2 mL of an aqueous 1 wt % thiolated PEG (6-mercaptohexan-PEG) solution was added into colloidal solutions to avoid agglomeration.

■ ASSOCIATED CONTENT

Ⓢ Supporting Information

X-ray crystallographic files and additional analytic data (crystal packing, NMR spectra, CHNS analytics, TEM-images) of all compounds and nanoparticles are available as Supporting Information. This material is available free of charge via the Internet at http://pubs.acs.org.

■ AUTHOR INFORMATION

Corresponding Author

*E-mail: sanjay.mathur@uni-koeln.de (S.M.).

Notes

The authors declare no competing financial interest.

■ ACKNOWLEDGMENTS

The authors are thankful to the University of Cologne for the financial and infrastructural support.

■ REFERENCES

(1) Edwards, P. P.; Thomas, J. M. *Angew. Chem., Int. Ed* **2007**, *46*, 5480−5486.
(2) Daniel, M.-C.; Astruc, D. *Chem. Rev.* **2004**, *104*, 293−346.
(3) (a) Faraday, M. *Philos. Trans. R. Soc. London* **1857**, *147*, 145−181. (b) Schmid, G. *Cluster and Colloids from Theory to Applications*; VCH: New York, 1994.
(4) Sondi, I.; Salopek-Sondi, N. *J. Colloid Interface Sci.* **2004**, *275*, 177−182.
(5) (a) Gorin, D. J.; Toste, F. D. *Nature* **2007**, *446*, 395−403. (b) Castro, E. G.; Salvatierra, R. V.; Schreiner, W. H.; Oliviera, M. M.; Zarbin, A. J. G. *Chem. Mater.* **2010**, *22*, 360−370. (c) Toshima, N.; Yoneshawa, T. *New J. Chem.* **1998**, *22*, 1179−1201. (d) Zopes, D.; von Hagen, R.; Müller, R.; Fiz, R.; Mathur, S. *Nanoscale* **2010**, *2*, 2091−2095.
(6) (a) Gianfranco, G.; Nicolais, F. *Materials* **2009**, *2*, 1323−1340. (b) Noguez, C. *J. Phys. Chem. C* **2007**, *111*, 3806−3819.
(7) Storhoff, J. J.; Lazarides, A. A.; Mucic, R. C.; Mirkin, C. A.; Letsinger, R. L.; Schatz, G. C. *J. Am. Chem. Soc.* **2000**, *122*, 4640−4650.
(8) Stark, W. J. *Angew. Chem.* **2011**, *123*, 1276−1293.
(9) Chen, D. H.; Chen, C. J. *J. Mater. Chem.* **2002**, *12*, 1557−1562.
(10) (a) Wang, A. Q.; Liu, J. H.; Lin, S. D.; Lin, T. S.; Mou, C. Y. *J. Catal.* **2005**, *233*, 186−197. (b) Wang, A. Q.; Chang, C. M.; Mou, C. Y. *J. Phys. Chem. B* **2005**, *109*, 18860−18867.
(11) Turkevich, J.; Stevenson, P. C.; Hillier, J. *J. Phys. Chem.* **1953**, *57*, 670−673.
(12) Link, S.; El Sayed, M. A. *J. Phys. Chem. B* **1999**, *103*, 8410−8426.
(13) Lee, P. C.; Meisel, D. *J. Phys. Chem.* **1982**, *86*, 3391−3395.
(14) Patel, K.; Kapoor, S.; Dave, D. P.; Mukherjee, T. *Res. Chem. Intermed.* **2006**, *32*, 103−113.
(15) Liu, S.; Chen, G.; Prasad, P. N.; Swihart, M. T. *Chem. Mater.* **2011**, *23*, 4098−4101.
(16) Huang, C.; Lai, W. C.; Tsai, C. Y.; Yang, C. H.; Yeh, C. S. *Chem.—Eur. J.* **2012**, *18*, 4107−4114.
(17) Luska, K. L.; Moores, A. *Can. J. Chem.* **2012**, *90*, 145−152.
(18) Ott, L. S.; Finke, R. G. *Coord. Chem. Rev.* **2007**, *251*, 1075−1100.
(19) Zopes, D.; Stein, B.; Mathur, S.; Graf, C. *Langmuir* **2013**, *29*, 11217−11226.
(20) Fischer, R. A. *Chem. Unserer Zeit* **1995**, *29*, 141−152.
(21) Mathur, S.; Shen, H. In *Encyclopedia of Nanoscience and Nanotechnology*; American Scientific Publisher: Stevenson Ranch, CA, 2004; Vol. 4, pp131−191.
(22) Zopes, D.; Kremer, S.; Scherer, H.; Belkhoura, L.; Pantenburg, I.; Tyrra, W.; Mathur, S. *Eur. J. Inorg. Chem.* **2011**, 273−280.
(23) Martinez-Salvador, S.; Fornies, J.; Martin, A.; Menjon, B. *Angew. Chem., Int. Ed.* **2011**, *50*, 6571−6574.

DOI: 10.1021/ic502924s
Inorg. Chem. 2015, 54, 3781−3787

(24) Donau, J. *Monatsh. Chem.* **1905**, *26*, 525−530.
(25) Altaf, M.; Stoeckli-Evans, H. *Polyhedron* **2009**, *29*, 701−708.
(26) Socol, S. M.; Jacobson, R. A.; Verkade, J. G. *Inorg. Chem.* **1984**, *23*, 88−94.
(27) Alyea, E. C.; Malito, J.; Nelson, J. H. *Inorg. Chem.* **1987**, *26*, 4294−4296.
(28) Goel, R. G.; Pilon, P. *Inorg. Chem.* **1978**, *17*, 2876−2879.
(29) Fernandez, E. J.; Laguna, A.; Lopez-de-Luzuriaga, J. M.; Monge, M.; Pyykkö, P.; Runeberg, N. *Eur. J. Inorg. Chem.* **2002**, 750−753.
(30) Zopes, D.; Hegemann, C.; Tyrra, W.; Mathur, S. *Chem. Commun.* **2012**, *48*, 8805−8807.
(31) Kleinmaier, R.; Arenz, S.; Karim, A.; Carlsson, A-C. C.; Erdelyi, M. *Magn. Reson. Chem.* **2013**, *51*, 46−53.
(32) Tyrra, W.; Naumann, D. *J. Fluorine Chem.* **2004**, *125*, 823−830.
(33) Jucker, K.; Sahm, W.; Schwenk, A. *Z. Naturforsch.* **1976**, *31a*, 1532−1538.
(34) Uson, R.; Laguna, A.; Laguna, M.; Jones, P. G.; Sheldrick, G. M. *J. Chem. Soc., Chem. Commun.* **1981**, 1097−1098.
(35) Massoud, A.; Langer, V.; Abu-Youssef, M. A. M. *Acta Crystallogr.* **2009**, *C65*, 352−354.
(36) Habiyakare, A.; Lucken, E. A. C.; Bernardinelli, G. *J. Chem. Soc., Dalton Trans.* **1991**, 2269−2273.
(37) Klabunde, K. J.; Campostrini, R. *J. Fluorine Chem.* **1989**, *42*, 93−104.
(38) Link, S.; Wang, Z. L.; El-Sayed, M. A. *J. Phys. Chem. B* **1999**, *103*, 3529−3533.
(39) Uppal, M. A.; Ewing, M. B.; Parkin, I. P. *Eur. J. Inorg. Chem.* **2011**, 4534−4544.
(40) Mulvaney, P. *Langmuir* **1996**, *12*, 788−800.
(41) *X-Shape 1.06*; Stoe and Cie GmbH: Darmstadt, Germany, 1999.
(42) *X-Area 1.16*; Stoe and Cie GmbH: Darmstadt, Germany, 2003.
(43) *X-RED 1.22*; Stoe and Cie GmbH: Darmstadt, Germany, 2001.
(44) Farrugia, L. J. *J. Appl. Crystallogr.* **1999**, *32*, 837−838.
(45) Altomare, A.; Cascarano, G.; Giacovazzo, C.; Guagliardi, A. *J. Appl. Crystallogr.* **1993**, *26*, 343−350.
(46) *SHELXL-97*; Universität Göttingen: Göttingen, Germany, 1997.

DOI: 10.1021/ic502924s
Inorg. Chem. 2015, 54, 3781−3787